JBIC (1997) 2:507–514

ORIGINAL ARTICLE

**Pedro M. Matias · José Morais · Ana V. Coelho
Rob Meijers · Ana Gonzalez · Andrew W. Thompson
Larry Sieker · Jean LeGall · Maria Arménia Carrondo**

A preliminary analysis of the three-dimensional structure of dimeric di-haem split-Soret cytochrome *c* from *Desulfovibrio desulfuricans* ATCC 27774 at 2.5-Å resolution using the MAD phasing method: a novel cytochrome fold with a stacked-haem arrangement

Received: 28 February 1997 / Accepted: 24 May 1997

Abstract Haem-containing proteins are directly involved in electron transfer as well as in enzymatic functions. The "split-Soret" cytochrome (SSC) was isolated from the sulfate- and nitrate-reducing bacterium *Desulfovibrio desulfuricans* ATCC 27774 and has no significant nitrate or nitrite reductase activity. The protein received its name due its unusual spectral properties. It is a dimer containing two identical subunits of 26.3 kDa, each with two haem-*c* groups. A preliminary model for the three-dimensional structure of this cytochrome was derived using the Multiple Wavelength Anomalous Dispersion (MAD) phasing method. This model shows that SSC is indeed a dimer containing four haems at one end of the molecule. In each monomer the two haems have their edges overlapped within van der Waals contacts with an iron-to-iron distance of 9 Å. The polypeptide chain of each monomer supplies the sixth axial ligand to the haems of the other monomer. This work shows that SSC constitutes a new class of cytochrome. The stacking of the two haems in the monomer within van der Waals distances of each other, and also the short (van der Waals) distances between the two monomers in the dimeric molecule are unprecedented in hemoproteins. This particular haem arrangement is an excellent model for the spectral study (undertaken several years ago) of haem-haem interaction using the aggregated haem undecapeptide derived from mammalian cytochrome *c*.

Key words Dimeric dihaem cytochrome · Stacked haem arrangement · MAD phasing · X-ray structure · Novel fold

P. M. Matias · J. Morais · A. V. Coelho · R. Meijers · L. Sieker
J. LeGall · M. A. Carrondo (✉)
Instituto de Tecnologia Química e Biológica, Universidade Nova de Lisboa, Apartado 127, P-2780 Oeiras, Portugal
Tel.: +351 1 4418215; Fax: +351 1 4411277;
e-mail: carrondo@itqb.unl.pt

A. V. Coelho
Chemistry Department, Universidade de Évora, P-7000 Évora, Portugal

A. W. Thompson
EMBL Grenoble Outstation, c/o ILL 20, BP-156, F-38042 Grenoble Cedex, France

A. Gonzalez[1]
ESFR, BP-220, F-38043 Grenoble Cedex, France

L. Sieker
Department of Biological Structure, University of Washington, Seattle, WA 98195, USA

Present address:
[1] EMBL, c/o DESY, Notkestrasse 85, D-22603 Hamburg, Germany

Supplementary material Refined atomic parameters for the Fe sites are available as Table S1 in electronic form on Springer Verlag's sever under: http://science.springer.de/jbic/jbic.htm

Introduction

A large variety of haem-containing proteins have been isolated from sulfate-reducing bacteria; these proteins include cytochromes which are directly involved in electron transfer as well as other haem-containing molecules with enzymatic functions. For recent comprehensive reviews, see [1].

The "split-Soret" cytochrome (SSC) was isolated from the sulfate- and nitrate-reducing bacterium *Desulfovibrio desulfuricans* ATCC 27774 (Dd_{27774}) and has not yet been found in any other organism. The protein received its trivial name from the observation that, upon reduction, not only was a maximum found at the unusual value for a cytochrome *c* of 424 nm for the Soret band, but also a shoulder appeared at 415 nm in the UV-visible spectrum [2].

SSC is a dimer with a molecular mass of 52.6 kDa, containing two identical subunits of 26.3 kDa. Each subunit contains two haem-*c* groups with bis-histidinyl iron axial co-ordination and distinct midpoint redox potentials of −168 (Haem 1) and −330 mV (Haem 2). The N-terminal sequence shows no homology with any other known cytochrome [3]. The physiological role of

the protein is still unknown, and the complete protein sequence is not yet available. It has no significant nitrate or nitrite reductase activities and is present in both sulfate- and nitrate-grown cells of Dd_{27774} [2]. Furthermore, its presence has not been detected in other ammonia-forming bacteria such as *Wollinella succinogenes* and *Escherichia coli.* Finally, a screening of the other strains of sulfate-reducing bacteria which are also capable of nitrate reduction remains to be made in order to find out whether the presence of SCC can be linked to this type of respiration. Here we present a report of the determination of a preliminary model for the three-dimensional structure of this cytochrome using the Multiple Wavelength Anomalous Dispersion (MAD) phasing method.

Material and methods

Rectangular prismatic crystals were first obtained from a 15 mg/ml protein solution using 17–19% (w/v) polyethylene glycol 8000 (PEG 8K) in 0.1 M sodium acetate buffer pH 5.0 by the sitting drop method at room temperature (ca. 20 °C). Only a small percentage were diffraction quality single crystals with many tending to be hollow. The reproducibility of good quality crystals was very low. The crystals also decayed rapidly when exposed to the X-ray beam. In order to overcome this problem, flash-freezing of the crystals was planned, but the crystals were found to be very sensitive to the addition of cryoprotecting compounds to the crystallization solution. Optimal diffraction quality crystals were finally obtained by crystallizing the protein from a solution containing 0.1–0.2% (w/v) agarose in 12–15% PEG 8K, 0.1 M sodium acetate buffer pH 5.0 which is essentially the same as mentioned above but containing the agarose. The agarose was prepared according to the protocol described by Robert, Provost and Lefaucheux [4] and was added to the crystallization solution. The presence of the agarose did not cause gelling of the crystallizing solution in the normal arrangement for crystallization, but there was an improvement in crystal quality, as reported in several papers [5–10], and the stability to X-rays was also dramatically improved. In addition, the crystals were no longer sensitive to the addition of the glycerol as a cryoprotecting agent. Best results were obtained by using 25% (v/v) glycerol. Crystallographic characterization was carried out using diffraction data collected at room temperature. Crystals belong to the orthorhombic space group $P2_12_12_1$ with cell dimensions $a = 98.2$ Å, $b = 100.5$ Å, $c = 110.6$ Å. Assuming four molecules (i.e., two dimers) in the asymmetric unit, the volume per unit of molecular weight (V_m) obtained is 2.59 Å^3/Da, corresponding to an estimated solvent content of 53%. This is within the normal range observed for protein crystals [11]. However, a self-rotation calculation failed to reveal any consistent set of peaks compatible with the presence of non-crystallographic symmetry axes.

Because of the difficulty in finding suitable heavy-atom derivatives, the MAD [12] method, using the Fe atoms in the native protein as anomalous scatterers, was considered for the determination of the three-dimensional structure of this protein. Synchrotron diffraction data were collected using a 180-mm MAR scanner at ESRF on bean line BM14 from a frozen crystal of SSC (dimensions $0.5 \times 0.3 \times 0.3$ mm^3) at three suitable wavelengths near the Fe absorption edge, chosen from an EXAFS scan of a frozen crystal (not shown): λ_1 1.7401 Å to maximise $\Delta f'$ (point of inflexion), λ_2 1.739 Å to maximize $\Delta f''$ (peak), and λ_3 1.6984 Å as the remote wavelength close to the edge. A fourth wavelength, λ_4 0.992 Å, was used as the scaling reference wavelength to facilitate scaling of the data by minimizing absorption problems which might be present at the other three wavelengths. The unit cell parameters at 100 K were $a = 96.06$ Å, $b = 100.13$ Å, $c = 109.30$ Å. The diffraction images were processed and scaled with the HKL suite [13, 14]. The scaling was carried out in such a way as to preserve the multiple observations of all the measured Bijvoet pair reflections. The CCP4 [15] program suite was then used to merge together the scaled data (ROTAPREP/AGROVATA), convert intensities to structure factors (TRUNCATE [16]) and to scale together the different wavelength data relatively to λ_4 (SCALEIT). The data collection, processing and scaling statistics are summarised in Table 1. While processing the fourth wavelength data it was realised that it suffered from a large number of saturated reflections, due to the much higher beam intensity at that wavelength for the exposure time per image chosen; this resulted in the loss of some low-to-medium resolution data. In order to overcome this problem, the λ_3 and λ_4 data were combined to produce a fifth data set which benefited from λ_3's completeness at low-to-medium resolution and from λ_4's completeness at the higher resolution. These data were later used in the calculation of electron density maps up to 2.5 Å resolution.

The anomalous difference Patterson map calculated from the data with maximal anomalous differences (λ_2 1.739 Å) showed clear peaks which could be interpreted in terms of three of the eight expected Fe sites, using RSPS [17]. The three Harker sections of this map are represented in Fig. 1. The remainder of the Fe sites were located by means of successive anomalous Fourier syntheses using the refined protein phases from the previously known and refined sites. The self- and cross-vectors arising from these sites that occur on or near the three Harker sections of the anomalous difference Patterson map, are clearly visible and

Table 1 Summary of data collection, processing and scaling statistics. Values in parentheses refer to the last resolution shell, $2.90 \geq d \geq 2.75$ Å for λ_1, λ_2 and λ_3, $2.63 \geq d \geq 2.50$ Å for λ_4, $3.56 \geq d \geq 2.50$ Å for $\lambda_3 + \lambda_4$. Scaling $R_{\text{factor}}(F) = \Sigma_{hkl}(F_{\lambda i} - F_{\lambda 4})/\Sigma_{hkl}F_{\lambda 4}$

Wavelength	λ_1, 1.7401 Å	λ_2, 1.739 Å	λ_3, 1.6984 Å	λ_4, 0.992 Å	$\lambda_3 + \lambda_4$
d_{min}, Å	19.9	19.9	19.9	19.7	19.9
d_{max}, Å	2.75	2.75	2.75	2.50	2.50
$N_{\text{observations}}$	106379	105131	107475	103858	212798
$N_{\text{reflections}}$	26134	26130	26239	28573	34228
% complete	94.3 (92.6)	94.3 (92.9)	94.7 (95.5)	78.3 (86.9)	93.1 (86.5)
multiplicity	4.1	4.0	4.1	3.6	6.2
R_{merge}	0.029 (0.080)	0.029 (0.080)	0.029 (0.079)	0.032 (0.070)	0.038 (0.074)
R_{anom}	0.025 (0.052)	0.037 (0.064)	0.030 (0.054)	0.023 (0.049)	N/A
$N_{\text{Bijvoet pairs}}$	22159	21990	22350	22112	N/A
% complete Bijvoet	80.0	79.4	80.7	60.6	N/A
$I/\sigma(I)$	17.5 (9.4)	18.2 (9.4)	17.5 (9.2)	21.4 (10.5)	9.7 (9.7)
Scaling $R_{\text{factor}}(F)$	0.053	0.053	0.029	–	N/A

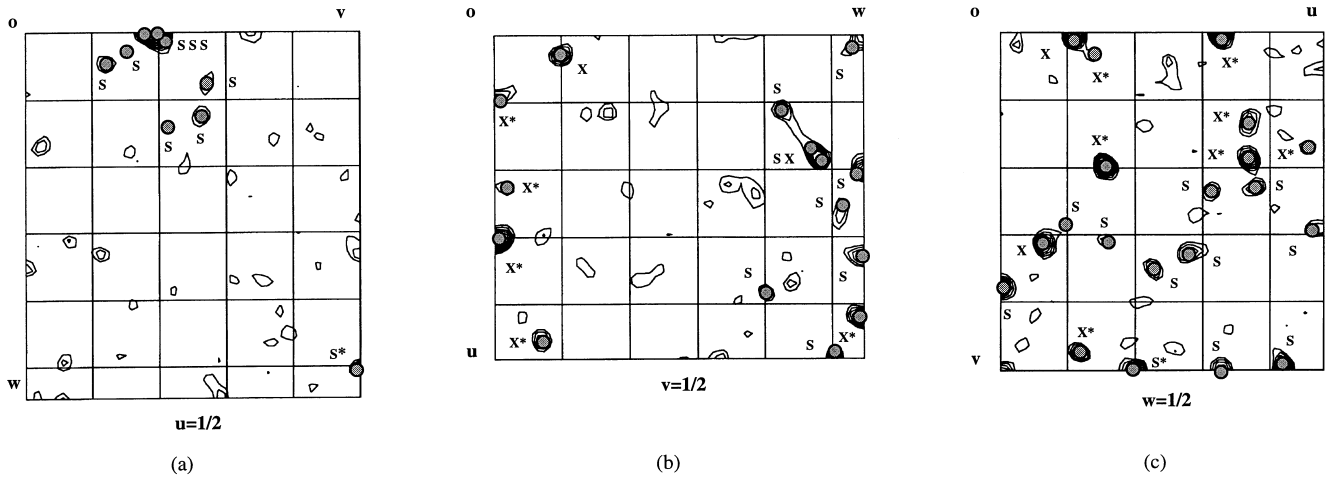

(a) (b) (c)

Fig. 1 Harker sections of the anomalous difference Patterson map calculated from λ_2 data. Contours are drawn at 1 map rms intervals, starting at 2 rms units. The shaded circles represent the predicted positions of the self- and cross-vectors arising from the Fe sites that occur on or near each Harker section. Self-vectors are labelled S, cross-vectors are labelled X. Peaks that occur in the section immediately above or below the Harker section are further labelled*

shown in Fig. 1. Only two sites have some self-vectors that do not match peaks in the map at the contouring levels shown. However, all of these sites refined satisfactorily. Phase refinement was carried out with MLPHARE [18] following a procedure previously described by Ramakrishnan et al. [19] and also by Glover et al. [20]. Taking the data set with largest $\Delta f'$ (λ_1) as the native with intrinsic anomalous scattering, the other data sets can be regarded as derivatives with "isomorphous" differences given by the dispersive differences $\Delta f'_i - \Delta f'_1$, each derivative having its own anomalous scattering. Furthermore, since the anomalous scatterers have full occupancy, using unit anomalous scattering factors will allow the explicit refinement of $\Delta f'_i - \Delta f'_1$ and $\Delta f''_i$ respectively as "isomorphous" and anomalous occupancies. These values will be expressed in electrons if the data have been placed on an absolute scale, which is only approximately true in this case. The advantage of using λ_1 as the native data set is that all "isomorphous" occupancies are then positive numbers. Phase refinement with MLPHARE in the resolution range $10 \geq d \geq 2.8$ Å converged to an overall figure of merit of 0.59. A summary of the phase refinement statistics is presented in Table 2, and the refined Fe atomic parameters are submitted as supplementary material. The refined Fe atomic positions were used to derive the non-crystallographic symmetry operations between the independent molecules (LSQKAB [21]). Selected non-crystallographic symmetry operators are listed in Table 3.

Density modification procedures (DM [22]), which included averaging, solvent flattening, histogram matching and phase extension ($20 \geq d \geq 2.5$ Å) using the structure factors from the fifth data set, obtained as described above, produced a much improved electron density map over that obtained from the original MAD phases. A model containing the haem groups and a polyalanine chain was built into this map using the graphics program O [23] corresponding to most of the polypeptide chain trace. All of the

Table 2 Summary of the MLPHARE phase refinement statistics

Wavelength	Phasing power acentric	Phasing power centric	Acentric R_{cullis}	Centric R_{cullis}	Anomalous R_{cullis}
λ_1	–	–	–	–	0.82
λ_2	0.50	0.43	0.94	0.91	0.70
λ_3	1.61	1.32	0.69	0.60	0.75
λ_4	1.85	1.51	0.63	0.57	0.89

Table 3 Non-crystallographic symmetry operations between the four independent SSC molecules

NCS operation[a]	Spherical polar angles (°)			Translation vector (Å)			rmsd (Å)[a]
	ω	ϕ	χ	T_x	T_y	T_z	
1→2[b]	134.22	−69.57	179.97	57.13	−27.40	46.88	0.082
1→3[b,c]	21.05	149.39	178.54	79.12	89.22	6.03	0.239
1→4[b]	81.54	10.45	73.61	10.88	125.24	22.14	0.232
3→4	149.82	83.20	179.98	84.76	170.51	104.27	0.066

[a] rmsd is the root mean square displacement between the two atomic sets being superimposed

[b] These NCS operators were used in the averaging calculations of the density modification procedure described in the text. To overcome the parameter indetermination in LSQKAB, the four Fe atoms in the dimer were used to derive the NCS operators

[c] This NCS operator is the same as that relating the two dimers in the asymmetric unit

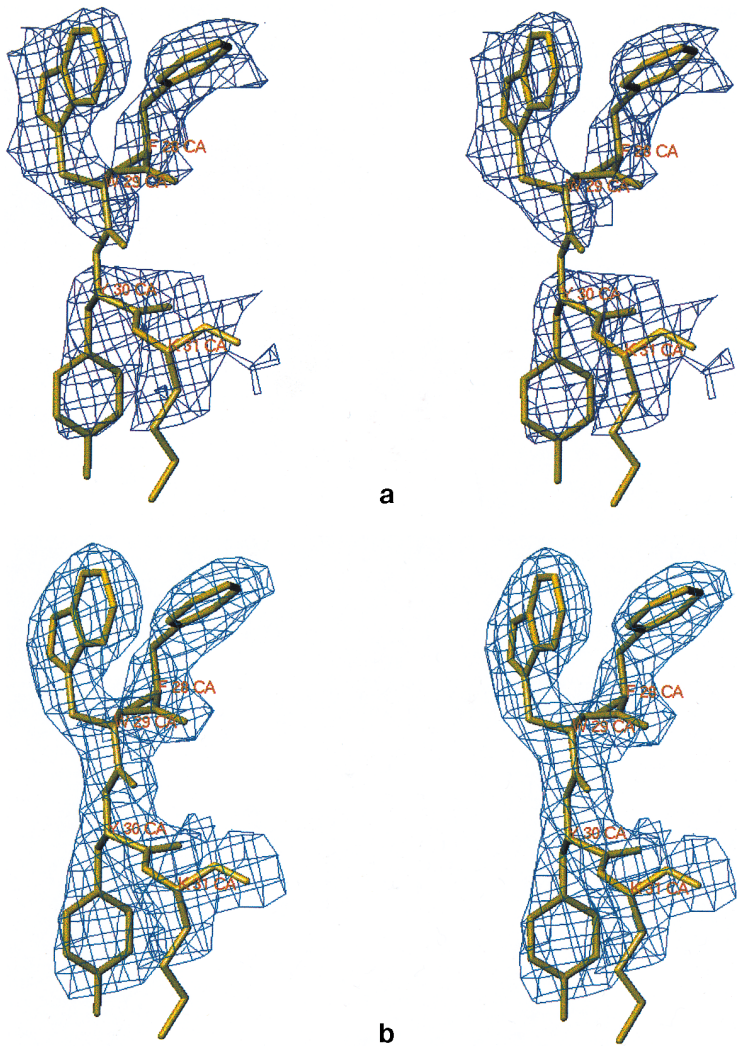

Fig. 2a, b Example of the improvement of the SSC electron density maps. Both maps are drawn at the 1 map rms level using TURBO [25]. **a** Map calculated using the MAD phases obtained from MLPHARE. **b** Map calculated using the phases obtained at the end of the density modification procedure as described in the text. The residues superimposed in the density do not reflect any sequence information but represent in the eyes of the crystallographer a reasonable fit to the electron density

sulfur atom positions in the cysteine residues attached to the haems could be seen in a 2.8-Å anomalous Fourier map, using the λ_2 anomalous differences as coefficients and the improved DM phases. This model was used for calculating phases which were then combined (SIGMAA [24]) with the original MAD/MLPHARE phases ($10 \geq d \geq 2.8$ Å) to produce a set of phases with an overall f.o.m. of 0.80. The density modification procedure was repeated ($20 \geq d \geq 2.5$ Å) to produce an improved electron density map. This map was of excellent quality and allowed a very nearly complete trace of the electron density; a model containing the haem groups and a polyalanine chain (including the cysteine and histidine residues bound to the haems) containing 235 residues was built. The improvement of the electron density maps is illustrated in Fig. 2.

The coordinates of the C^{α} and haem group atoms of the SSC monomer have been deposited in the Protein Data Bank [26, 27] with accession code 1ddc.

Results and discussion

This paper describes a preliminary model of SSC, highlighting the success of the MAD technique in a situation with eight independent anomalous scatterers, (4 monomers, each with 2 haem iron atoms per asymmetric unit, and where the iron is a relatively weak anomalous scatterer when compared with, e.g., selenium). In addition, a novel fold has been found together with a unique arrangement of the haem groups. Full details of the complete structure determination are not described herein, because technical reasons, including the limited synchrotron beam time available for the total experiment, prevented the re-collection of the λ_4 data and the collection of diffraction data to a resolution better than 2.5 Å. Furthermore, the reproducible growth of high-quality crystals has proved difficult. When this problem can be overcome, high-resolution data will be collected, a full crystallographic refinement undertaken and a complete analysis of the resulting structural model reported.

Model description

The C^{α} trace of the preliminary model of the three-dimensional structure of SSC is represented in Fig. 3. The monomer contains 235 residues plus two haem groups, and there are four monomers in the asymmetric unit. The two monomers in each dimer are related by a

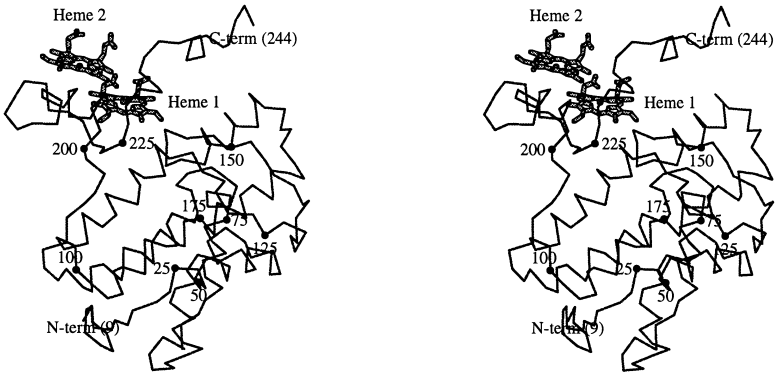

Fig. 3 MOLSCRIPT [28] stereo diagram of the C^{α} trace of the model for the three-dimensional structure of the SSC monomer

non-crystallographic twofold rotation axis, and the two adjacent dimers are likewise related by a non-crystallographic twofold rotation axis (see Table 3). The arrangement for the SSC dimer is shown as a MOLSCRIPT [28] diagram in Fig. 4.

The tracing of the present model as a polyalanine chain was possible by using the electron density maps obtained as described in Materials and methods. The contiguous electron density is consistent with a number of residues compatible with the monomer molecular weight of 26.3 kDa although there is evidence in the electron density maps that there may be a few more residues at both termini. The unambiguous polarity of the α-helices located in the structure, combined with the fact that the dimers are very well resolved in the electron density maps, as well as the tracing restrictions imposed by the presence of a non-crystallographic twofold rotation axis in each dimer allow us to attribute a considerable degree of confidence to the model now proposed.

To our knowledge, the three-dimensional structure of SSC constitutes a new cytochrome fold. A search in the Protein Data Bank [26, 27] was carried out using the EMBL Dali server (http://www.embl-heidelberg.de/dali/dali.html) [29] and failed to reveal any significantly similar protein folds.

The haem groups are attached to one end of the protein and exposed to the solvent, rather than being wrapped by the polypeptide chain as is the case in the other known cytochrome structures. Indeed, the protein can almost be regarded as being constituted of two parts, the haem-binding region and a domain which contains nine α-helices, one of which is seven turns long and runs across this domain. On the basis of the electron density alone, it is possible to confirm that both haems have histidines as the axial ligands and both are covalently attached to the polypeptide chain through cysteinyl thioether linkages. Also, the haem-binding motif is clearly C-X-X-C-H, as found in many other cytochrome molecules, and there are 15 residues separating the two haem-binding motifs. Fig. 5 shows the histidine and cysteinyl linkages to each of the haems in the SSC monomer. One unusual characteristic exhibited by this structure is that the axial coordination of the Fe atom in each haem group is completed by a histidine residue supplied by the other monomer in the dimer, as shown in Figs. 4 and 5. This observation has the implication that the dimer is indeed the functional unit of SSC. In the inner haem (less exposed to solvent) the histidine imidazole rings are nearly perpendicular to each other, while in the outer haem (more exposed to solvent) they are close to being coplanar (see Figs. 4 and 5).

These results are in agreement with the hypothesis of Walker et al. [30], which states that haems with EPR signal g_{max} greater than 3 have the planes of their two histidine ligands perpendicular to each other. The EPR results obtained by Costa [31] show g_{max} values of 3.44 for Haem 1 (inner haem) and of 2.98 for Haem 2 (outer haem). Since Haem 1 has the highest redox value ($E° = -168$ mV at pH 7.6) whereas Haem 2 has the lowest value ($E° = -330$ mV at same pH) [3], the model is also in agreement with Stellwagen [32], who predicted that a haem with more exposure to solvent should have a lower redox potential.

Figure 5 shows that the electron density clouds of the two haem groups are nearly parallel, stacking on top of each other, and the closest distance between them is 4 Å. In the dimer, the four haem groups are in close proximity, and the haems from each monomer are only slightly tilted with respect to the haems of the adjacent monomer. The independent distances between haem iron atoms in the SSC molecule are represented in Fig. 6. It should be noted that these conclusions are based on the experimental electron density map, but are not expected to change significantly when knowledge of the primary structure of SSC and higher-resolution data will allow the building of a complete structural model.

Comparison with di-haem proteins

In other di-haem proteins the haems occurring in two separate domain structures are arranged so that the angle between the haem planes varies considerably, from almost 30° in the case of cytochrome c_4 [33, 34] and flavocytochrome *c* sulfide dehydrogenase [35], 60° in cytochrome cd_1 nitrite reductase [36], and 90° in cytochrome *c* peroxidase [37]. However, the distances sepa-

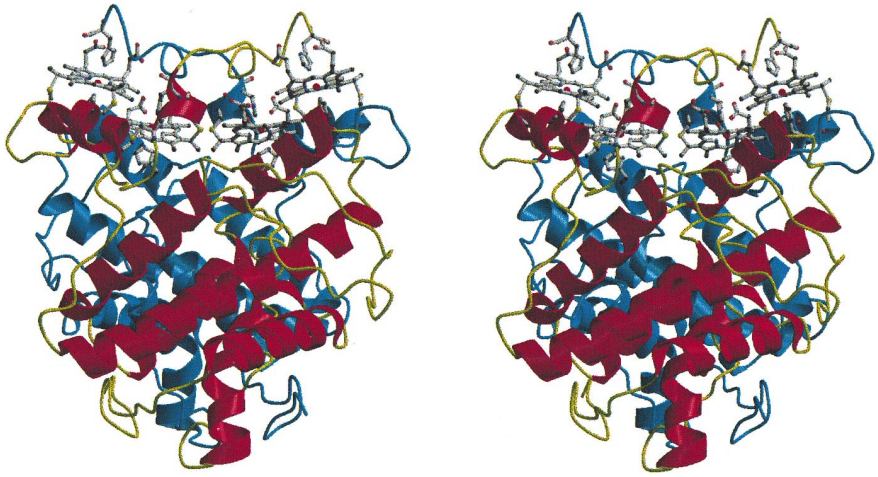

Fig. 4 MOLSCRIPT [28] stereo diagram of the SSC dimer. The foreground monomer is represented in two colours (*red* for helices, *yellow* for coils/loops) and the background monomer in *cyan*. The haems and the cysteine and histidine residues attached to them are represented in ball-and-stick mode. The NCS 2-fold axis is approximately vertical and in the plane of the page. This diagram is drawn in the same orientation as Fig. 3

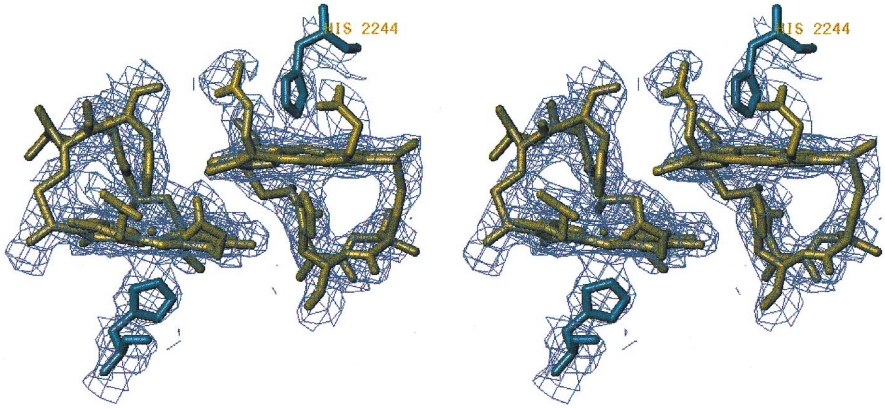

Fig. 5 Stereoview of the two haem groups in the SSC monomer, showing the C-X-X-C-H binding motifs as well as the other histidine residue, which comes from the second monomer. The outer haem is located on the *right*, the inner haem on the *left*. The superimposed electron density was drawn at the 1 rms contour level. Drawing made with TURBO [25]

rating the iron atoms appear to be somewhat similar in all these molecules, being in the range 16 to 21 Å.

In the case of SSC, the two haems from each monomer are in the same region and are nearly parallel. However, and perhaps more importantly, the distance between the haem-iron atoms in each monomer is only about 9 Å, and the haems are nearly stacked on one another, the closest distance between the haem rings being only 4 Å. These distances are much shorter than those found in any of the other di-haem molecules. Furthermore, in the SSC dimeric molecule the four haems form a compact cluster arrangement at an extreme end of the molecule.

Another structural characteristic related to the function of some of these di-haem molecules is worth a close comparison with what is seen in SSC. In cytochrome cd_1 the axial coordination of the d_1 haem is accomplished via a histidine and a tyrosine residue. However this axial Tyr25 is supplied by the extension of the loop of chain from the C-terminal domain. The proposed mechanism for the enzymatic activity of this protein is that the reduction of the enzyme causes the removal of this axial ligand so that nitrite or oxygen may bind to the iron atom of the d_1 haem.

In the case of cytochrome *c* peroxidase, the low-potential haem has both histidine residues as axial ligands. One is well buried inside the molecule while the second sits on the tip of a flexible loop on the surface of the molecule. The catalytic activity of this enzyme is suggested to be related to movement of the latter histidine, allowing peroxide binding.

A very interesting similar feature exists in the SSC molecule but involves both haem groups. Each haem has an axial histidine supplied by the neighbouring subunit. The most exposed haem in SSC has a histidine coming from the C-terminal chain of the other monomer, on the surface of the dimeric molecule (see Fig. 4). The second, more internal, haem also has an axial histidine supplied by another segment of the adjacent subunit. It is possible that at least one of these histidines can move in a similar manner to that proposed for cytochromes *cd* and *c* peroxidase.

Some other interesting aspects

It is also important to point out that the tetrahaem arrangement found in the SSC bears no resemblance to the tetrahaem clusters found in cytochromes c_3, including that from the same organism [38]. In the cytochromes c_3 none of the haems are within van der Waals distance of one another and the four haems have all their ligands from the same polypeptide chain. The eight haems in the dimeric c_3 of *Desulfomicrobium ba-*

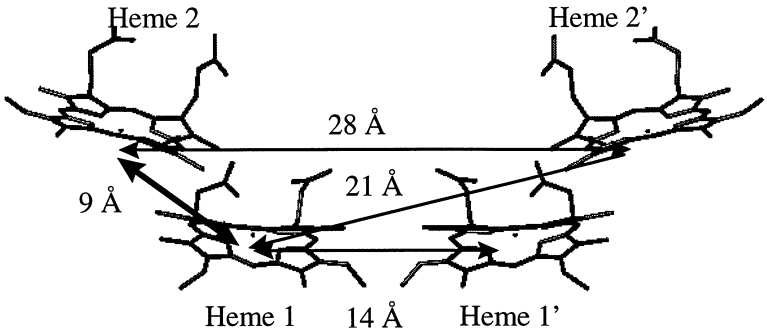

Fig. 6 Diagram showing the independent distances between the four haem iron atoms in the SSC molecule. The haems are numbered according to [3]. Drawing made with TURBO [25]

culatus strain Norway 4, formerly known as *D. desulfuricans* Norway [39] have, in each monomer, the same arrangement as the typical c_3 structure. However, the interaction at the dimer interface also shows a close approach between haems.

This exceptional haem packing in the structure of SSC provides a first example in nature of the artificial assembly of haem stacking in the so-called haem undecapeptide from mammalian cytochrome *c*; the latter has been studied as a model system for the interaction of haem moieties in more complex biological systems. This peptide can be obtained by peptic digestion of the protein yielding a haem-containing peptide [40, 41], and was known to aggregate [42]. This aggregate showed interesting splitting and red-shifting of the Soret band [43]. The optical spectra of the aggregated form, both in the ferrous and ferric forms, show striking similarities to SSC [2]. Furthermore, Urry [43] speculated that the haems in the aggregated undecapeptide were likely stacked in a head-to-tail alignment rather than in a card-packing fashion, with a distance between haem centres of 9–10 Å: these conclusions are remarkably in agreement with the haem arrangement in SSC.

Conclusions

The structure of SSC presented herein reveals that this dimeric hemoprotein constitutes a new class of cytochrome. In particular this molecule has the interesting feature of the two dihaem-containing monomers with haems in an almost parallel, stacked arrangement, associating so that the adjoining pair of haems are within van der Waals distances of each other. These features are unprecedented in the haemproteins whose structures have so far been determined. Furthermore, each haem has its sixth axial ligand supplied by the polypeptide chain of the other monomer, in a comparable manner to that found in other dihaem-containing proteins with enzymatic activity. This close haem arrangement provides an excellent natural model for understanding the splitting of the Soret band.

Acknowledgements This work was funded by JNICT grant PMCT/C/BIO 874/90 and European Union grants BIO2-CT942052 and HCM-CHRX-CT93-0143. Rob Meijers was supported by an Erasmus grant (PIC-NL-1067). The authors would like to thank Prof. A. V. Xavier for helpful discussions and encouragement, Dr. Kevin Cowtan (University of York, UK) for his invaluable help with the density-modification calculations involving non-crystallographic symmetry averaging, the fermentation plant at University of Georgia, Athens, G, USA for growing the bacteria, Profs. J. J. G. Moura and I. Moura, Dr. Cristina Costa and Dr. M.-Y. Liu for the purified protein sample used for crystallization, and the EMBL (Grenoble) for support. Diffraction data were collected at beamline BM14 and the ESRF (Grenoble).

References

1. Peck HD Jr, LeGall J (eds) (1994) Inorganic microbial sulfur metabolism. (Methods in Enzymology, vol. 243) Academic Press, New York
2. Liu M-C, Costa C, Coutinho IB, Moura JJG, Moura I, Xavier AV, LeGall J (1988) J Bacteriol 170:5545–5551
3. Moura JJG, Costa C, Liu M-Y, Moura I, LeGall J (1991) Biochim et Biophys Acta 1058:61–66
4. Robert MC, Provost K, Lefaucheux F (1992) In: Ducruix A, Giegé R (eds) Crystallization of nucleic acids and proteins. Oxford University Press, Oxford, pp 127–142
5. Cudney B, Patel S, McPherson A (1994) Acta Cryst D50:479–483
6. García-Ruiz JM, Moreno A (1994) Acta Cryst D50:484–490
7. Thiessen KJ (1994) Acta Cryst D50:491–495
8. Robert MC, Bernard Y, Lefaucheux F (1994) Acta Cryst D50:496–503
9. Bernard Y, Degoy S, Lefaucheux F, Robert MC (1994) Acta Cryst D50:504–507
10. Sica F, Demasi D, Mazzarella L, Zagari A, Capasso S, Pearl LH, D'Auria S, Raia CA, Rossi M (1994) Acta Cryst D50:508–511
11. Matthews BW (1968) J Mol Biol 33:491–497
12. Hendrickson WA (1991) Science 254:51–58
13. Minor W (1993) XDISPLAYF Program. Purdue University, West Lafayette, Indiana, USA
14. Otwinowski Z (1993) In: Sawyer L, Isaacs N, Bailey S (eds) Proceedings of the CCP4 Study Weekend: Data collection and processing. SERC Daresbury Laboratory UK, pp 56–62
15. Collaborative Computational Project Number 4 (1994) Acta Cryst D50:760–763
16. French GS, Wilson KS (1978) Acta Cryst A34:517–525
17. Knight S (1989) Ph D thesis. Swedish University of Agricultural Sciences, Uppsala, Sweden
18. Otwinowski Z (1991) In: Wolf W, Evans PR, Leslie AGW (eds) Proceedings of the CCP4 Study Weekend: Isomorphous refinement and anomalous scattering. SERC Daresbury Laboratory, UK, pp 80–86
19. Ramakrishnan V, Finch JT, Graziano V, Lee PL, Sweet RM (1993) Nature (London) 362:219–223
20. Glover I, Denny RC, Nguti ND, McSweeney S, Kinder SH, Thompson AW, Dodson EJ, Wilkinson AJ, Tame JRH (1995) Acta Cryst D51:39–47
21. Kabsch W (1976) Acta Cryst A32:922–923

22. Cowtan K (1994) In: Winn M (ed) Joint CCP4 and ESF-EACBM Newsletter on Protein Crystallography Number 31, SERC Daresbury Laboratory, UK, pp 34–38
23. Jones TA, Zou JY, Cowan SW, Kjeldgaard M (1991) Acta Cryst A47:110–119
24. Read RJ (1986) Acta Cryst A42:140–149
25. Roussel A, Fontecilla-Camps JC, Cambillau C (1990) TURBO-FRODO: A new program for protein crystallography and modelling. XV IUCR Congress, Bordeaux, France
26. Abola EE, Bernstein FC, Bryant SH, Koetzle TF, Weng J (1987) In: Allen FH, Bergeroff G, Sievers R (eds) Crystallographic databases – information content, software systems, scientific applications. Data Commission of the International Union of Crystallography, Bonn, Cambridge, Chester, pp 107–132
27. Bernstein FC, Koetzle TF, Williams GJB, Meyer EF Jr, Brice MD, Rodgers JR, Kennard O, Shimanouchi T, Tasumi M (1977) J Mol Biol 112:535–542
28. Kraulis PJ (1991) J Appl Cryst 24:946–950
29. Holm L, Sander, C (1993) J Mol Biol 233:123–138
30. Walker FA, Huynh BH, Scheidt, WR, Osvath SR (1986) J Am Chem Soc 108:5288–5297
31. Costa C (1994) PhD dissertation. Universidade Nova de Lisboa, Portugal
32. Stellwagen E (1978) Nature 275:73–74
33. Kadziola A, Larsen S (1997) Structure 5:203–216
34. Moore GR, Pettigrew GW (1990) Cytochromes *c*: evolutionary, structural and physicochemical Aspects. Springer, Berlin Heidelberg New York
35. Chen Z, Koh M, Gonzalez VD, Van Beeumen JJ, Bartsch RG, Meyer TE, Cusanovitch MA, Mathews FS (1994) Science 266:430–432
36. Fülöp V, Moir JWB, Ferguson SJ, Hajdu J (1995) Cell 81:369–377
37. Fülöp V, Ridout CJ, Greenwood C, Hajdu J (1995) Structure 3:1225–1233
38. Morais J, Palma PN, Frazão C, Caldeira J, LeGall J, Moura I, Moura JJG, Carrondo MA (1995) Biochemistry 34:12830–12841
39. Czjzek M, Guerlesquin F, Bruschi M, Haser R (1996) Structure 4:395–404
40. Tsou CL (1951) Biochem J 49:362–374
41. Tuppy H, Paléus S (1955) Acta Chem Scand 9:353–364
42. Paléus S, Ehrenberg A, Tuppy H (1955) Acta Chem Scand 9:365–374
43. Urry DW (1967) J Am Chem Soc 89:4190–4196
44. Czjzek M, Payan F, Guerlesquin F, Bruschi M, Haser R (1994) J Mol Biol 243:653–667
45. Matias PM, Morais J, Coelho R, Carrondo MA, Wilson K, Dauter Z, Sieker L (1996) Prot Sci 5:1342–1354
46. Louro RO, Catarino T, Salgueiro CA, LeGall J, Xavier AV (1996) JBIC 1:34–38